

Semi-supervised multi-organ segmentation via multi-planar co-training

Yuyin Zhou¹, Yan Wang¹, Peng Tang^{1,2},
Wei Shen^{1,3}, Elliot K. Fishman⁴, Alan L. Yuille¹

¹The Johns Hopkins University, Baltimore, MD 21218, USA

²Huazhong University of Science and Technology, Wuhan 430074, China

³Shanghai University, Baoshan District, Shanghai 200444, China

⁴The Johns Hopkins University School of Medicine, Baltimore, MD 21287, USA
zhouyuyiner@gmail.com wyanny.9@gmail.com tangpeng723@gmail.com
wei.shen@t.shu.edu.cn efishman@jhmi.edu alan.l.yuille@gmail.com

Abstract. Multi-organ segmentation is a critical problem in medical image analysis due to its great value for computer-aided diagnosis, computer-aided surgery, and radiation therapy. Although fully-supervised segmentation methods can achieve good performance, they usually require a large amount of 3D data, such as CT scans, with voxel-wised annotations which are usually difficult, expensive, and slow to obtain. By contrast, large unannotated datasets of CT images are available. Inspired by the well-known semi-supervised learning framework co-training, we propose multi-planar co-training (MPCT), to generate more reliable pseudo-labels by enforcing consistency among multiple planes, i.e., sagittal, coronal, and axial planes, of 3D unlabeled medical data, which play a vital role in our framework. Empirical results show that generating pseudo-labels by the multi-planar fusion rather than a single plane leads to a significant performance gain. We evaluate our approach on a new collected dataset and show that MPCT boosts the performance of a typical segmentation model, fully convolutional networks, by a large margin, when only a small set of labeled 3D data is available, i.e., 77.49% vs. 73.14%.

1 Introduction

Multi-organ segmentation of radiology images is a critical task which is essential to many clinical applications such as computer-aided diagnosis and computer-aided surgery. Compared with other internal human anatomical structures like brain or heart, abdominal organs appear to be much more challenging due to the low contrast and high variability of shape in CT images. In this paper, we focus on the problem of multi-organ segmentation in the abdominal region (e.g., liver, pancreas, kidney, etc.).

Recent advances in deep learning [7] have brought great benefit to the biomedical imaging domain. Specially, fully convolutional networks (FCNs) [8] have been widely applied to many biomedical segmentation tasks such as neuronal

structures segmentation [3,4,11,14], single-organ segmentation [12,15], and multi-organ segmentation [13].

The methods mentioned above train their segmentation networks in fully supervised settings which require a large amount of labeled data. However, labeling medical images is extremely difficult, time consuming, and laborious, even for experienced radiologists. By contrast, unlabeled medical data are much easier and cheaper to obtain. How to make use of extra unlabeled data to train segmentation networks, i.e., training networks in semi-supervised settings, such as EM algorithms [9,16], is a promising direction to explore.

To this end, we propose an EM-like semi-supervised learning method under the co-training framework [2], named multi-planar co-training, for multi-organ segmentation in CT images. Here, we take the fact that a CT volume can be reconstructed from different planes, i.e., sagittal, coronal, and axial planes. Our goal is to use all the planes together to allow unlabeled data to augment labeled data. More specifically, multiple networks are trained on the multiple planes of labeled data separately, and then the network predictions from multiple planes are fused to generate pseudo-labels for the unlabeled data and thus enlarging the training set. This fusion module is able to generate more reliable pseudo-labels for unlabeled data than just using one plane. Benefited from this, our method outperforms other semi-supervised segmentation methods which are trained on each single plane separately.

2 Multi-planar Co-training

We propose multi-planar co-training (MPCT), a semi-supervised multi-organ segmentation method which exploits multi-planar information to generate pseudo-labels for unlabeled 3D CT volumes. Assume that we are given a 3D CT volume dataset \mathcal{S} containing K organs. This includes labeled volumes $\mathcal{S}_L = \{(\mathbf{I}_m, \mathbf{Y}_m)\}_{m=1}^l$ and unlabeled volumes $\mathcal{S}_U = \{\mathbf{I}_m\}_{m=l+1}^M$, where \mathbf{I}_m and \mathbf{Y}_m denote a 3D input volume and a ground-truth segmentation mask, respectively, l and $M-l$ are the number of labeled and unlabeled volumes, respectively, and typically $l \ll M$. MPCT involves the following steps:

- **Step 1:** train a *teacher model* on the manually labeled data \mathcal{S}_L in the fully supervised setting as in Sec. 2.1;
- **Step 2:** assign pseudo-labels $\{\hat{\mathbf{Y}}_m\}_{m=l+1}^M$ to the unlabeled data \mathcal{S}_U by fusing the estimations from all planes as in Sec. 2.2;
- **Step 3:** train a *student model* on the union of the manually labeled data and automatically labeled data $\mathcal{S}_L \cup \{(\mathbf{I}_m, \hat{\mathbf{Y}}_m)\}_{m=l+1}^M$ as in Sec. 2.3.
- **Step 4:** perform step 2 & 3 in an iterative manner.

The overall pipeline is demonstrated in Figure 1.

2.1 Teacher model

We train the teacher model on the labeled dataset \mathcal{S}_L . By splitting each volume and its corresponding label mask in the sagittal (S), coronal (C) and axial (A)

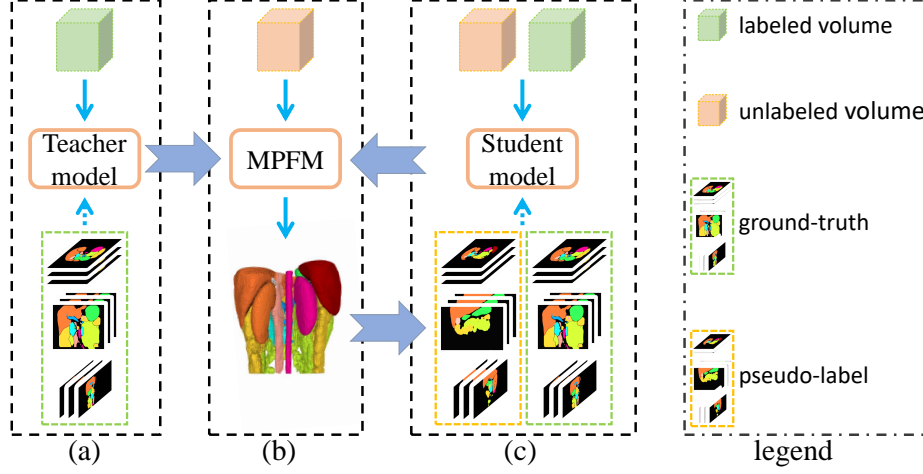


Fig. 1. Illustration of the multi-planar co-training (MPCT) framework. (a) We first train a teacher model on the labeled dataset. (b) We then use the teacher model to assign pseudo-label to the unlabeled data using our multi-planar fusion module (MPFM) as demonstrated in Figure 2. (c) Finally, we train a student model over the union of both the labeled and the unlabeled data. Step (b) and (c) are performed in an iterative manner.

planes, we can get 3 sets of 2D slices, i.e., $\mathcal{S}_L^V = \{\mathbf{I}_n^V, \mathbf{Y}_n^V\}_{n=1}^{N_V}$, $V \in \{S, C, A\}$, where N_V is the number of 2D slices obtained from plane V . We train a 2D-FCN model (we use [8] as our reference CNN model throughout this paper) to perform segmentation from each plane individually.

Without loss of generality, let $\mathbf{I}^V \subset \mathbb{R}^{W \times H}$ and $\mathbf{Y}^V = \{y_i^V\}_{i=1}^{W \times H}$ denote a 2D slice and its corresponding label mask in \mathcal{S}_L^V , where $y_i^V \in \{0, 1, \dots, K\}$ is the organ label (0 means background) of the i -th pixel in \mathbf{I}^V . Consider a segmentation model $\mathbb{M}^V : \hat{\mathbf{Y}} = \mathbf{f}(\mathbf{I}^V; \boldsymbol{\Theta})$, where $\boldsymbol{\Theta}$ denotes the model parameters, $\hat{\mathbf{Y}}$ denotes the prediction for \mathbf{I}^V . Our objective function is:

$$\mathcal{L}(\mathbf{I}^V, \mathbf{Y}^V; \boldsymbol{\Theta}) = -\frac{1}{W \times H} \left[\sum_{i=1}^{W \times H} \sum_{k=0}^K \mathbb{1}(y_i^V = k) \log p_{i,k}^V \right], \quad (1)$$

where $p_{i,k}^V$ denotes the probability of the i -th pixel been classified as label k on 2D slice \mathbf{I}^V and $\mathbb{1}(\cdot)$ is the indicator function. We train the teacher model by optimizing \mathcal{L} w.r.t. $\boldsymbol{\Theta}$ by stochastic gradient descent.

2.2 pseudo-label generation

Given a well-trained teacher model $\{\mathbb{M}^V | V \in \{S, C, A\}\}$, our goal is to generate the pseudo-label $\{\hat{\mathbf{Y}}_m\}_{m=l+1}^M$ for the unlabeled data \mathcal{S}_U .

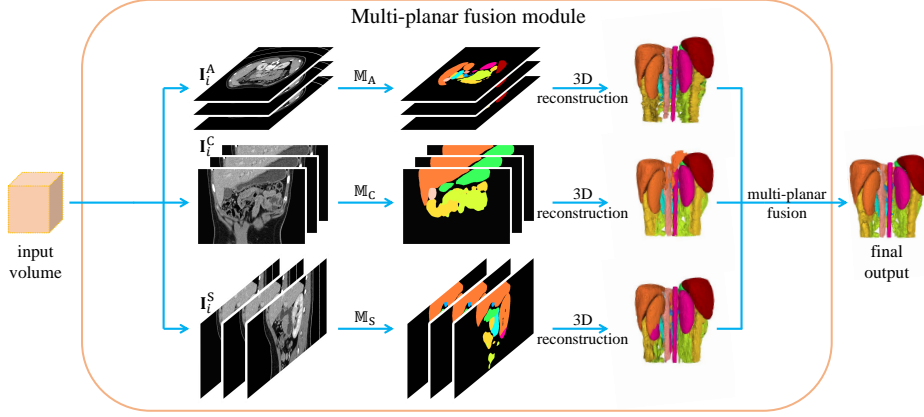


Fig. 2. Illustration of Multi-planar fusion module (MPFM), where the input 3D volume is first parsed into 3 set of slices along sagittal, coronal, and axial planes to be evaluated respectively. The final 3D estimation is obtained by fusing the predictions from each individual plane.

We first make predictions on the 2D slices from each plane and then reconstruct the 3D volume by stacking all slices back together. Previous studies [6,10] suggest that combining predictions can often improve the accuracy and the robustness of the final decision. Therefore, the fused prediction from multiple planes is better than any estimation of a single plane.

More specifically, we first adopt the “Vote Rule” to fuse the hard estimations by seeking agreement among different planes. If the predictions from all planes do not agree on a voxel, then we select the prediction for that voxel with the maximum confidence. Other rules [1] can also be easily adapted to this module. We do not focus on discussing the influence of the fusion module in this paper, but intuitively better fusion module should lead to higher performance. The final decision for the i -th voxel y_i^* of $\hat{\mathbf{Y}}_m$ is computed by:

$$y_i^* = \begin{cases} y_i^V, & \text{if } \exists V, V' \in \{S, C, A\}, V \neq V' \mid y_i^V = y_i^{V'}, \\ y_i^{V^*}, & \text{otherwise} \end{cases}, \quad (2)$$

where $V^* = \arg \max_{V \in \{S, C, A\}} \max_j p_{i,j}^V$. $p_{i,j}^S$, $p_{i,j}^C$, and $p_{i,j}^A$ denote the probabilities of the i -th pixel classified as label j from the sagittal, coronal, and axial planes, respectively. y_i^V denotes the hard estimation for the i -th pixel on view V , i.e., $y_i^V = \arg \max_j p_{i,j}^V$.

2.3 Student model

After generating the pseudo-labels $\{\hat{\mathbf{Y}}_m\}_{m=l+1}^M$ for the unlabeled dataset \mathcal{S}_U , the training set can be then enlarged by taking the union of both the labeled

Algorithm 1 Multi-planar co-training for multi-organ segmentation

Input: A set of labeled data $\mathcal{S}_L = \{(\mathbf{I}_m, \mathbf{Y}_m)\}_{m=1}^L$ and unlabeled volumes $\mathcal{S}_U = \{\mathbf{I}_m\}_{m=L+1}^M$.

Output: A trained multi-organ segmentation model $\{\mathbb{M}^S, \mathbb{M}^C, \mathbb{M}^A\}$.

$\mathcal{S} \leftarrow \mathcal{S}_L$

for $t = 1$ to T **do**

Parse \mathcal{S} into $\mathcal{S}^S, \mathcal{S}^C, \mathcal{S}^A$.

Train $\mathbb{M}^S, \mathbb{M}^C$, and \mathbb{M}^A on $\mathcal{S}^S, \mathcal{S}^C$, and \mathcal{S}^A respectively.

Generate pseudo-class labels $\{\hat{\mathbf{Y}}_m\}_{m=L+1}^M$ for the unlabeled dataset \mathcal{S}_U by Eq. 2

Augment the training set by adding the self-labeled examples to \mathcal{S} , i.e., $\mathcal{S} = \mathcal{S}_L \cup \{(\mathbf{I}_m, \hat{\mathbf{Y}}_m)\}_{m=L+1}^M$.

end for

Parse \mathcal{S} into $\mathcal{S}^S, \mathcal{S}^C, \mathcal{S}^A$.

Train $\mathbb{M}^S, \mathbb{M}^C$, and \mathbb{M}^A on $\mathcal{S}^S, \mathcal{S}^C$, and \mathcal{S}^A respectively.

and the unlabeled dataset, i.e., $\mathcal{S} = \mathcal{S}_L \cup \{(\mathbf{I}_m, \hat{\mathbf{Y}}_m)\}_{m=L+1}^M$. The student model is trained on this augmented dataset \mathcal{S} the same way we train the teacher model as described in Sec. 2.1.

The overall training procedure is summarized in Algorithm 1. In the training stage, we first train a teacher model in a supervised manner and then use it to generate the pseudo-labels for the unlabeled dataset. Then we alternate the training of the student model and the pseudo-label generation procedures in an iterative manner to optimize the student model T times. In the testing stage, we follow the method in Sec. 2.2 to generate the final estimation using the T -th student model.

3 Experiments

3.1 Dataset and Evaluation

Our fully-labeled dataset includes 210 contrast-enhanced abdominal clinical CT images in the portal venous phase, in which we use a random split of 100/30/80 patients for training, validation, and testing. Our unlabeled dataset consists of 100 unlabeled cases. Each CT volume consists of $319 \sim 1051$ slices of 512×512 pixels, and have voxel spatial resolution of $([0.523 \sim 0.977] \times [0.523 \sim 0.977] \times 0.5)mm^3$. The validation set is used to determine the hyperparameters for training, e.g., training iterations. The metric we use is the Dice-Sørensen Coefficient (DSC), which measures the similarity between the prediction voxel set \mathcal{Z} and the ground-truth set \mathcal{Y} , with the mathematical form of $DSC(\mathcal{Z}, \mathcal{Y}) = \frac{2 \times |\mathcal{Z} \cap \mathcal{Y}|}{|\mathcal{Z}| + |\mathcal{Y}|}$. We report the average DSC scores together with the standard deviation over all testing cases.

3.2 Implementation details

We set the learning rate to be 10^{-9} . During each iteration, we train the teacher model for 80K iterations and the student model for 160K iterations. Similar to

Table 1. Segmentation accuracy, i.e., DSC (%), of 16 abdominal organs by different approaches using varying number of labeled and unlabeled data. See Section 3.3 for definitions of “supervised”, “SPSL”, and “MPCT”.

Organ	Method	supervised	SPSL		MPCT	
	$\frac{\# \text{unlabeled}}{\# \text{labeled}}$	0	50	100	50	100
Aorta	50	89.14 ± 7.95	91.10 ± 5.49	90.76 ± 5.87	91.43 ± 4.85	91.54 ± 4.65
	100	90.25 ± 7.58	91.37 ± 5.09	90.99 ± 5.39	90.90 ± 5.88	90.91 ± 5.55
Adrenal gland	50	26.45 ± 12.07	29.92 ± 14.65	26.93 ± 15.46	30.58 ± 12.65	35.48 ± 11.76
	100	36.44 ± 12.01	32.66 ± 13.34	36.47 ± 12.63	35.22 ± 12.13	38.96 ± 10.83
Celiac AA	50	33.70 ± 20.46	35.88 ± 19.78	38.29 ± 19.47	34.90 ± 21.15	38.98 ± 20.01
	100	36.09 ± 20.07	39.34 ± 19.51	38.44 ± 20.60	39.89 ± 19.23	40.11 ± 19.45
Colon	50	70.92 ± 16.84	77.30 ± 15.47	78.59 ± 15.48	78.61 ± 15.02	79.52 ± 14.62
	100	78.96 ± 14.64	78.67 ± 15.17	78.43 ± 15.02	78.56 ± 14.94	78.78 ± 14.88
Duodenum	50	54.89 ± 15.54	57.77 ± 17.23	62.22 ± 14.75	66.95 ± 12.48	64.78 ± 13.79
	100	63.98 ± 13.82	64.50 ± 13.37	65.26 ± 13.51	62.27 ± 14.69	63.34 ± 14.25
Gall-bladder	50	82.21 ± 19.81	83.48 ± 19.75	82.37 ± 17.63	86.53 ± 14.73	85.88 ± 15.18
	100	83.97 ± 19.67	84.95 ± 17.48	82.60 ± 17.40	84.82 ± 17.54	83.70 ± 19.92
IVC	50	77.67 ± 9.49	81.28 ± 8.82	82.63 ± 7.27	83.49 ± 6.89	83.43 ± 7.02
	100	82.59 ± 7.02	83.04 ± 6.67	83.26 ± 7.10	83.24 ± 7.30	82.77 ± 7.21
Kidney_L	50	95.12 ± 5.01	95.59 ± 4.94	95.88 ± 3.66	95.82 ± 3.58	96.09 ± 3.42
	100	95.62 ± 3.52	95.74 ± 3.94	95.88 ± 3.52	95.74 ± 4.51	95.93 ± 4.05
Kidney_R	50	94.50 ± 10.89	94.57 ± 11.64	94.94 ± 11.00	94.96 ± 10.96	95.06 ± 10.93
	100	94.89 ± 10.89	94.73 ± 11.13	94.83 ± 11.27	94.81 ± 11.21	94.97 ± 11.22
Liver	50	95.45 ± 2.41	96.06 ± 0.98	96.07 ± 1.03	96.11 ± 0.96	96.15 ± 0.92
	100	96.04 ± 1.04	96.04 ± 0.97	96.10 ± 1.01	96.07 ± 1.06	96.03 ± 1.06
Pancreas	50	76.49 ± 11.63	80.12 ± 7.48	80.93 ± 6.80	81.46 ± 6.27	82.03 ± 6.16
	100	81.98 ± 6.18	81.52 ± 6.43	81.55 ± 6.45	81.38 ± 6.49	81.62 ± 6.29
SMA	50	51.61 ± 18.00	51.16 ± 18.90	51.29 ± 17.81	48.78 ± 19.72	52.04 ± 18.52
	100	45.57 ± 20.28	51.26 ± 18.18	51.06 ± 18.52	52.19 ± 19.53	54.53 ± 17.56
Small-bowel	50	71.13 ± 13.10	78.93 ± 12.54	79.97 ± 12.73	79.49 ± 12.03	79.25 ± 12.55
	100	79.78 ± 12.67	79.20 ± 12.73	79.23 ± 12.64	80.34 ± 12.49	80.30 ± 12.65
Spleen	50	94.81 ± 2.64	95.46 ± 2.08	95.58 ± 1.88	95.68 ± 2.03	95.98 ± 1.59
	100	95.63 ± 2.07	95.74 ± 1.92	95.71 ± 2.09	95.68 ± 2.04	95.76 ± 1.85
Stomach	50	91.38 ± 3.94	92.62 ± 3.69	92.92 ± 3.63	92.90 ± 3.80	93.42 ± 3.21
	100	93.27 ± 3.60	93.34 ± 3.48	93.40 ± 3.37	92.90 ± 3.83	93.06 ± 3.54
Veins	50	64.75 ± 15.39	70.43 ± 14.19	69.66 ± 14.51	69.82 ± 14.38	70.23 ± 14.42
	100	69.45 ± 14.52	69.33 ± 14.35	69.99 ± 14.31	69.31 ± 14.63	71.06 ± 14.36
Mean	50	73.14 ± 11.57	75.73 ± 11.10	76.19 ± 10.56	76.75 ± 10.07	77.49 ± 9.92
	100	76.53 ± 10.60	76.96 ± 10.27	77.08 ± 10.30	77.08 ± 10.53	77.61 ± 10.31

[5], we use three windows of $[-125, 275]$, $[-160, 240]$, and $[-1000, 1000]$ Housefield units to rescale each slice to $[0.0, 1.0]$. We initialize the network parameters Θ by using the FCN-8s model [8] pre-trained on the PascalVOC image segmentation dataset. The number of iterations for the alternating training is set to 2, i.e., $T = 2$ in Algorithm 1.

3.3 Results

Table 1 compares the multi-organ segmentation performance of our proposed MPCT approach with two baseline approaches: supervised learning method which only utilizes labeled data for training (“supervised” in the table) and single-planar based semi-supervised learning approach that performs semi-supervised learning on each single plane separately (“SPSL” in the table). It shows that if

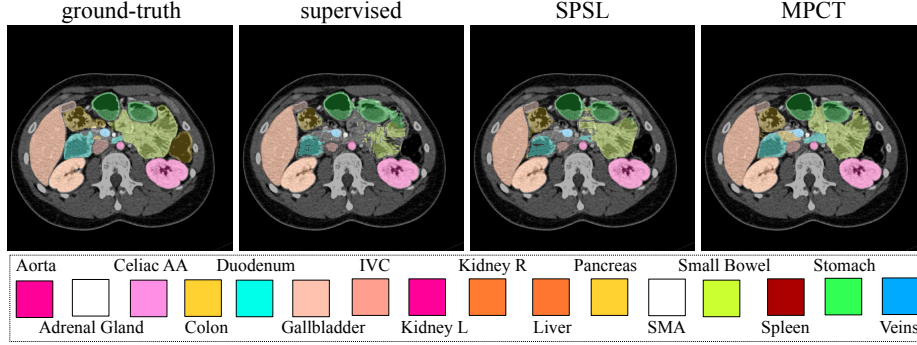


Fig. 3. For left to right are examples from ground-truth, fully-supervised method result, SPSL method result, and our MPCT method result. 50 labeled cases are used for all methods. 100 unlabeled cases are used for the SPSL and MPCT method. Our MPCT obtains better results than both the fully-supervised method and SPSL method especially in some hard organs, e.g., small bowel. See Section 3.3 for definitions of “supervised”, “SPSL”, and “MPCT”. Best viewed in color.

the same number of labeled data is used, semi-supervised learning generally improves performance. Compared with the fully supervised setting, adding 100 unlabeled cases to 50 labeled cases by using SPSL increases the average Dice score from $73.14\% \pm 11.57\%$ to $76.19\% \pm 10.56\%$, while using MPCT can boost the performance even further to $77.49\% \pm 9.92\%$. When there are more labeled data, i.e. 100 cases, the semi-supervised methods still obtain better performance than the supervised method, while the performance gain becomes less prominent. This is probably due to the fact that the ratio of unlabeled data to labeled data decreases. We believe that if more unlabeled data can be provided the performance should go up considerably. In addition, we find that our method outperforms both baselines, i.e., fully-supervised method and SPSL in every setting, which further demonstrates the usefulness of multi-planar fusion during co-training.

We also show a visualization of one case in Figure 3, which also proves that our proposed MPCT outperforms SPSL and even further outperforms the fully-supervised approach especially for some hard organs like small-bowel, which is also demonstrated in Table 1. We find that our MPCT can boost the segmentation performance of some hard organs such as pancreas (5.54%), colon (8.60%), duodenum (9.89%), and veins (5.48%). This promising result indicates that our method distills a reasonable amount of knowledge from unlabeled data.

4 Conclusions

In this paper, we proposed MPCT for multi-organ segmentation in abdominal CT scans, which is motivated by the original co-training strategy to incorporate

multi-planar information for the unlabeled data during training. We evaluate our approach on our own newly collected high-quality dataset. The results show that our method outperforms the fully-supervised learning approach by a large margin. In addition, our multi-planar based approach outperforms the single-planar method, which further demonstrates the benefit from multi-planar fusion. We also show that our model can learn better if more unlabeled data provided especially when the number of labeled data is small. We believe that our algorithm can achieve even higher accuracy if a more powerful network backbone or an advanced fusion algorithm is employed, which we leave as the future work.

References

1. Asman, A.J., Landman, B.A.: Non-local statistical label fusion for multi-atlas segmentation. *Medical image analysis* 17(2), 194–208 (2013)
2. Blum, A., Mitchell, T.: Combining labeled and unlabeled data with co-training pp. 92–100 (1998)
3. Chen, H., Qi, X., Cheng, J.Z., Heng, P.A., et al.: Deep contextual networks for neuronal structure segmentation. In: *AAAI*. pp. 1167–1173 (2016)
4. Ciresan, D., Giusti, A., Gambardella, L., Schmidhuber, J.: Deep Neural Networks Segment Neuronal Membranes in Electron Microscopy Images. *Advances in Neural Information Processing Systems* (2012)
5. Harrison, A.P., Xu, Z., George, K., Lu, L., Summers, R.M., Mollura, D.J.: Progressive and multi-path holistically nested neural networks for pathological lung segmentation from ct images. In: *International Conference on Medical Image Computing and Computer-Assisted Intervention*. pp. 621–629. Springer (2017)
6. Heckemann, R.A., Hajnal, J.V., Aljabar, P., Rueckert, D., Hammers, A.: Automatic anatomical brain mri segmentation combining label propagation and decision fusion. *NeuroImage* 33(1), 115–126 (2006)
7. Krizhevsky, A., Sutskever, I., Hinton, G.E.: Imagenet classification with deep convolutional neural networks. In: *Advances in Neural Information Processing Systems*. pp. 1097–1105 (2012)
8. Long, J., Shelhamer, E., Darrell, T.: Fully Convolutional Networks for Semantic Segmentation. In: *Proceedings of the IEEE Conference on Computer Vision and Pattern Recognition* (2015)
9. Papandreou, G., Chen, L.C., Murphy, K.P., Yuille, A.L.: Weakly-and semi-supervised learning of a deep convolutional network for semantic image segmentation. In: *Proceedings of the IEEE international conference on computer vision*. pp. 1742–1750 (2015)
10. Rohlfing, T., Brandt, R., Menzel, R., Maurer Jr, C.R.: Evaluation of atlas selection strategies for atlas-based image segmentation with application to confocal microscopy images of bee brains. *NeuroImage* 21(4), 1428–1442 (2004)
11. Ronneberger, O., Fischer, P., Brox, T.: U-Net: Convolutional Networks for Biomedical Image Segmentation. *International Conference on Medical Image Computing and Computer-Assisted Intervention* (2015)
12. Roth, H., Lu, L., Farag, A., Sohn, A., Summers, R.: Spatial Aggregation of Holistically-Nested Networks for Automated Pancreas Segmentation. *International Conference on Medical Image Computing and Computer-Assisted Intervention* (2016)

13. Roth, H.R., Oda, H., Hayashi, Y., Oda, M., Shimizu, N., Fujiwara, M., Misawa, K., Mori, K.: Hierarchical 3d fully convolutional networks for multi-organ segmentation. arXiv preprint arXiv:1704.06382 (2017)
14. Shen, W., Wang, B., Jiang, Y., Wang, Y., Yuille, A.: Multi-stage multi-recursive-input fully convolutional networks for neuronal boundary detection. arXiv preprint arXiv:1703.08493 (2017)
15. Zhou, Y., Xie, L., Shen, W., Wang, Y., Fishman, E.K., Yuille, A.L.: A fixed-point model for pancreas segmentation in abdominal ct scans. In: International Conference on Medical Image Computing and Computer-Assisted Intervention. pp. 693–701. Springer (2017)
16. Zhu, X.: Semi-supervised learning literature survey (2005)